UNIVERSITY OF AMSTERDAM

UvA-DARE (Digital Academic Repository)

CHIME/Slow Overview and Pilot Survey

A New Backend to Search for Second-duration Radio Transients with the CHIME Telescope

Mate, Sujay; Luke, Kevin; Bhusare, Yash; Balasubramanian, Arvind; Pleunis, Ziggy; Scholz, Paul; Tendulkar, Shriharsh P.; Bhardwaj, Mohit; Brar, Charanjot; Dong, Fengqiu Adam; Fonseca, Emmanuel; Gaensler, B.M.; Hessels, Jason; Huang, Jeff; Jain, Naman; Joseph, Ronniy C.; Kaspi, Victoria M.; Khan, Afrokk; Main, Robert; Meyers, Bradley W.; Milutinovic, Nikola; Nimmo, Kenzie; Shin, Kaitlyn; Spear, David; Stairs, Ingrid; Tan, Chia Min

DOI
10.3847/1538-4357/ae8847

Publication date
2026

Document Version
Final published version

Published in
Astrophysical Journal

License
CC BY

Link to publication

Citation for published version (APA):
Mate, S., Luke, K., Bhusare, Y., Balasubramanian, A., Pleunis, Z., Scholz, P., Tendulkar, S. P., Bhardwaj, M., Brar, C., Dong, F. A., Fonseca, E., Gaensler, B. M., Hessels, J., Huang, J., Jain, N., Joseph, R. C., Kaspi, V. M., Khan, A., Main, R., ... Tan, C. M. (2026). CHIME/Slow Overview and Pilot Survey: A New Backend to Search for Second-duration Radio Transients with the CHIME Telescope. *Astrophysical Journal*, *1008*(1), Article 55. https://doi.org/10.3847/1538-4357/ae8847

General rights
It is not permitted to download or to forward/distribute the text or part of it without the consent of the author(s) and/or copyright holder(s), other than for strictly personal, individual use, unless the work is under an open content license (like Creative Commons).

Disclaimer/Complaints regulations
If you believe that digital publication of certain material infringes any of your rights or (privacy) interests, please let the Library know, stating your reasons. In case of a legitimate complaint, the Library will make the material inaccessible and/or remove it from the website. Please Ask the Library: https://uba.uva.nl/en/contact, or a letter to: Library of the University of Amsterdam, Secretariat, P.O. Box 19185, 1000 GD Amsterdam, The Netherlands. You will be contacted as soon as possible.

UvA-DARE is a service provided by the library of the University of Amsterdam (https://dare.uva.nl)

Download date:17 Nov 2026

The Astrophysical Journal, 1008:55 (12pp), 2026 September 1 https://doi.org/10.3847/1538-4357/ae8847
© 2026. The Author(s). Published by the American Astronomical Society.
OPEN ACCESS

CHIME/Slow Overview and Pilot Survey: A New Backend to Search for Second-duration Radio Transients with the CHIME Telescope

Sujay Mate[1,2], Kevin Luke[3], Yash Bhusare[4], Arvind Balasubramanian[1,5], Ziggy Pleunis[6,7], Paul Scholz[8], Shriharsh P. Tendulkar[1,4], Mohit Bhardwaj[9], Charanjot Brar[10], Fengqiu Adam Dong[8,11], Emmanuel Fonseca[12,13], B. M. Gaensler[14,15,16], Jason Hessels[6,7,17,18], Jeff Huang[17,18], Naman Jain[17,18], Ronniy C. Joseph[17,18], Victoria M. Kaspi[17,18], Afrokk Khan[17,18], Robert Main[17,18], Bradley W. Meyers[19,20], Nikola Milutinovic[21], Kenzie Nimmo[22], Kaitlyn Shin[23], David Spear[21], Ingrid Stairs[21], and Chia Min Tan[20]
[1] Department of Astronomy and Astrophysics, Tata Institute of Fundamental Research, Mumbai, 400005, India; sujay.mate@rrimail.rri.res.in, sujay.mate@gmail.com
[2] Raman Research Institute, C. V. Raman Avenue, Sadashivanagar, Bangalore, Karnataka, 560080, India
[3] LUX, Observatoire de Paris, Université PSL, Sorbonne Université, CNRS, 92190 Meudon, France
[4] National Centre for Radio Astrophysics, Post Bag 3, Ganeshkhind, Pune, 411007, India
[5] Indian Institute of Astrophysics, Koramangala II Block, Bangalore 560034, India
[6] Anton Pannekoek Institute for Astronomy, University of Amsterdam, Science Park 904, 1098 XH Amsterdam, The Netherlands
[7] ASTRON, the Netherlands Institute for Radio Astronomy, Oude Hoogeveensedijk 4, 7991 PD Dwingeloo, The Netherlands
[8] Department of Physics and Astronomy, York University, 4700 Keele Street, Toronto, ON MJ3 1P3, Canada
[9] Department of Space Planetary Astronomical Sciences and Engineering, Indian Institute of Technology, KanpuR, Uttar Pradesh, India
[10] NRC Herzberg Astronomy and Astrophysics, 5071 West Saanich Road, Victoria, BC V9E2E7, Canada
[11] National Radio Astronomy Observatory, 520 Edgemont Road, Charlottesville, VA 22903, USA
[12] Department of Physics and Astronomy, West Virginia University, PO Box 6315, Morgantown, WV 26506, USA
[13] Center for Gravitational Waves and Cosmology, West Virginia University, Chestnut Ridge Research Building, Morgantown, WV 26505, USA
[14] Department of Astronomy and Astrophysics, University of California, Santa Cruz, 1156 High Street, Santa Cruz, CA 95060, USA
[15] Dunlap Institute for Astronomy and Astrophysics, 50 St. George Street, University of Toronto, ON M5S 3H4, Canada
[16] David A. Dunlap Department of Astronomy and Astrophysics, 50 St. George Street, University of Toronto, ON M5S 3H4, Canada
[17] Department of Physics, McGill University, 3600 rue University, Montréal, QC H3A 2T8, Canada
[18] Trottier Space Institute, McGill University, 3550 rue University, Montréal, QC H3A 2A7, Canada
[19] Australian SKA Regional Centre (AusSRC), Curtin University, Kent Street, Bentley, WA 6102, Australia
[20] International Centre for Radio Astronomy Research (ICRAR), Curtin University, Kent Street, Bentley, WA 6102, Australia
[21] Department of Physics and Astronomy, University of British Columbia, 6224 Agricultural Road, Vancouver, BC V6T 1Z1, Canada
[22] Center for Interdisciplinary Exploration and Research in Astronomy, Northwestern University, 1800 Sherman Avenue, Evanston, IL 60201, USA
[23] Division of Physics, Mathematics, and Astronomy, California Institute of Technology, Pasadena, CA 91125, USA
Received 2026 February 13; revised 2026 June 26; accepted 2026 July 1; published 2026 August 25

Abstract

We present an overview of CHIME/Slow, a real-time transient search backend under development to search for second-duration radio transients using the CHIME telescope, and results obtained from a pilot survey carried out using the prototype version of the search pipeline. The prototype CHIME/Slow pipeline was tested on archival data obtained in 2022 December, 2023 January, and 2023 February with a total on-sky time of 17 days with an instantaneous field of view of $\sim$13 deg^2. In this pilot survey, we detected nine bursts, one from a new nonrepeating source, FRB 20230204C, and eight from the known hyperactive repeating source FRB 20220912A. Out of these nine bursts, two bursts from the repeater were not detected by CHIME/FRB, while the nonrepeater was detected in the side-lobe of a beam in CHIME/FRB, exhibiting shorter burst width and narrower bandwidth compared to the CHIME/Slow detection. Here we report properties of the bursts, discuss the sensitivity and completeness of the current version of the CHIME/Slow pipeline, and outline future development to improve its performance. Finally, based on these results, we report the all-sky rate (95% credible region) of radio transients with burst widths between 16 ms and 5 s, fluence above 5 Jy ms, and observing frequency of 600 MHz to be between 184 and 4556 bursts sky^{-1} day^{-1}.

Unified Astronomy Thesaurus concepts: Radio transient sources (2008); Transient detection (1957); Radio interferometers (1345)

1. Introduction

The construction of radio interferometers with large mapping speeds (combining field of view and sensitivity) has led to a proliferation of radio transient detections in recent years. The detection of a large population of fast radio bursts (FRBs) through untargeted surveys (e.g., CHIME/FRB Collaboration et al. 2021) has led to many insights into this mysterious source class, but most instruments lack sensitivity to the widest and most highly scattered (timescales $\gtrsim$100 ms) bursts.

Radio transients associated with compact objects span a broad range in the burst width–luminosity phase space (Figure 1). FRBs and pulsars lie in the short-duration ($\sim$ms) region of the phase space, with FRBs occupying the extreme luminosity end. At much longer timescales ($\sim$minutes to days), emissions associated with active galactic nuclei, gamma-ray bursts (GRBs), and X-ray binaries are observed.

Original content from this work may be used under the terms of the Creative Commons Attribution 4.0 licence. Any further distribution of this work must maintain attribution to the author(s) and the title of the work, journal citation and DOI.

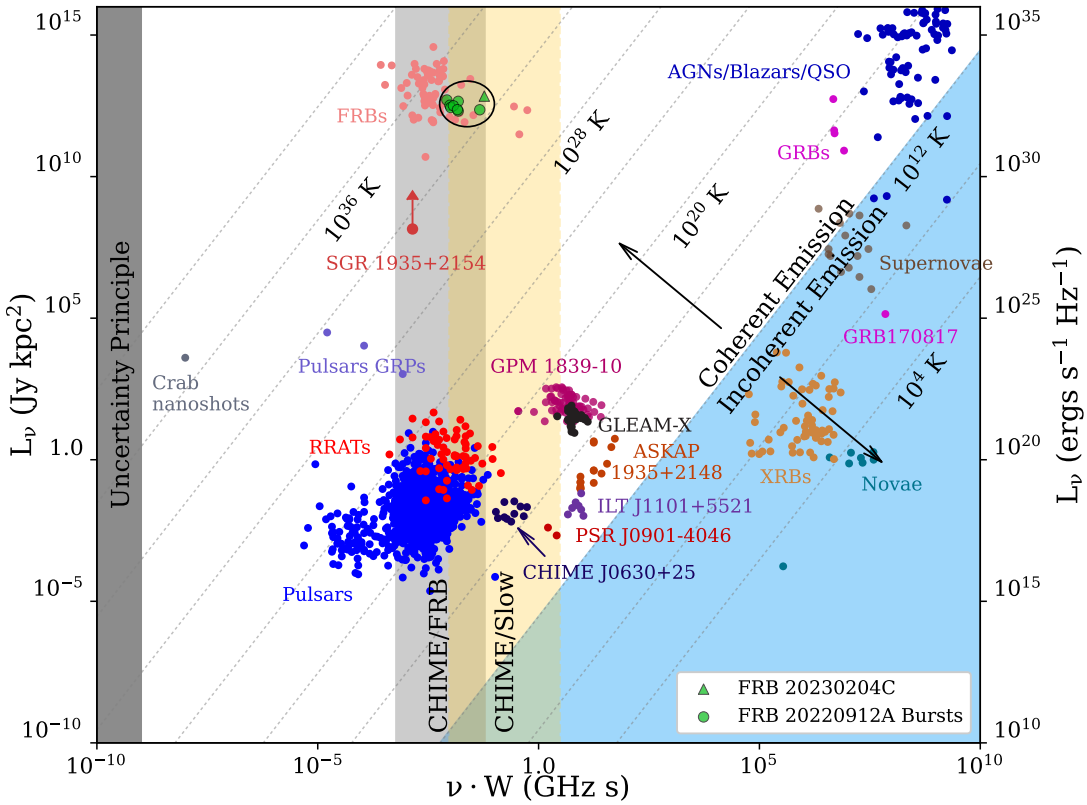

Figure 1. Radio transients associated with compact objects in the pseudoluminosity vs. pseudopulse width parameter space. The parts of the parameter space covered by CHIME/FRB and CHIME/Slow are highlighted in light gray and light yellow colors, respectively. The green points near the FRB population show the CHIME/Slow detections from the pilot survey with the circles indicating bursts from FRB 20220912A and the triangle indicating the nonrepeating burst FRB 20230204C (see Section 3 for more details). Figure adapted from J. M. Cordes et al. (2004) and E. F. Keane (2018) with data from N. Hurley-Walker et al. (2022, 2023), M. Caleb et al. (2022, 2024), F. A. Dong et al. (2025), I. de Ruiter et al. (2025), and this work. Note that the shaded regions only mark the widths covered.

However, only a handful of transients have been observed at ∼seconds duration, leaving a large gap in phase space. One of the reasons for a dearth of second-timescale transients has been primarily due to two technological limitations: the lack of gain stability of radio telescopes at these timescales for time-domain searches due to radio frequency interference (RFI) and bright sources transiting through sidelobes, and the computational challenge of doing image plane searches at very high (seconds) time resolution. However, recent advances in technology have allowed telescopes like the MeerKAT, Murchison Widefield Array (MWA), Canadian Hydrogen Intensity Mapping Experiment (CHIME), Australian Square Kilometre Array Pathfinder (ASKAP), and LOw Frequency ARray (LOFAR) to detect second-duration radio transients over the past few years. These mostly include long-period pulsar-like transients (LPTs) with pulse widths ranging from a few hundreds of milliseconds to a few tens of seconds (e.g., see M. Caleb et al. 2022, 2024; N. Hurley-Walker et al. 2022, 2023; I. de Ruiter et al. 2025; F. A. Dong et al. 2025).[24] The sources of these transients are still unknown, with some observations suggesting a neutron star/magnetar origin while other systems seem to be comprised of magnetized white dwarfs or interacting white dwarfs in binaries. Detailed follow-up observations and more detections of such LPTs are needed to understand this new class of sources.

Apart from these detections, some theories propose that compact binary mergers involving at least one neutron star could produce FRB-like flashes that could last for a few hundred milliseconds to a few seconds (e.g., see A. Rowlinson & G. E. Anderson 2019; N. Sridhar et al. 2021; M. Lyutikov 2024). Furthermore, it has been theorized that classical GRBs could also produce a radio flash of similar duration concurrent with the prompt emission if certain emission pathways dominate the GRB jet (i.e., if the jet is "Poynting flux" dominated, see V. V. Usov & J. I. Katz 2000). Several efforts have been made to search for FRB-like emission associated with compact binary mergers and GRBs, but none have resulted in a confirmed detection (M. M. Anderson et al. 2018; A. Rowlinson et al. 2019, 2021; R. L. C. Starling et al. 2020; J. Tian et al. 2022; S. I. Chastain et al. 2023; A. P. Curtin et al. 2023, 2024; A. Hennessy et al. 2023). However, these results are consistent given the search timescales, sky coverage, and sensitivity of these searches, and hence more systematic efforts are warranted. The CHIME/Slow backend, described below, will systematically search for second-timescale radio transients and aims to fill the as-yet largely unexplored parameter space.

This article is structured in the following way: Section 2 describes the CHIME/Slow pipeline and its major components. Section 3 presents the results from the pilot survey carried out using the prototype version of the CHIME/Slow pipeline. Section 4 describes the injection and completeness analysis performed to estimate the sensitivity of the current version of the CHIME/Slow pipeline, which is also used to estimate the all-sky rate of second-duration radio transients in Section 5. Section 6

[24] Full list of all-known LPTs with references can be found here: https://lpt.mwa-image-plane.cloud.edu.au/published/tables/1.

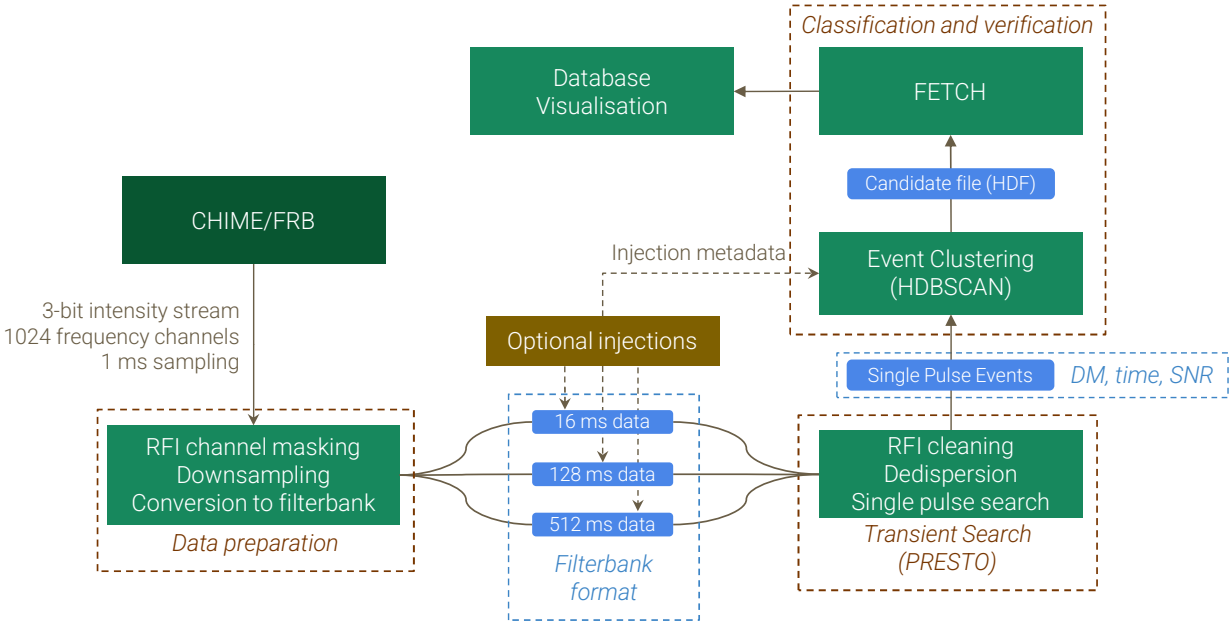

Figure 2. Overview of the CHIME/Slow pipeline: the diagram shows the major steps in the pipeline and the tools used to perform these steps. The light green blocks represent data processing routines, the blue blocks represent data products that are created during the search, and the brown block represents the injection subpackage.

discusses the implications of these results and future plans for the CHIME/Slow backend. Finally, Section 7 presents the summary and conclusions of this work. The Appendix describes additional details about the all-sky rate estimation.

2. The CHIME/Slow Backend

The CHIME/FRB backend (CHIME/FRB Collaboration et al. 2018) searches for FRBs with burst widths up to 100 ms and DMs up to 13,000 pc cm^{-3}. The upper limits on the burst widths and DMs were decided as a compromise between computational cost and statistical optimization to search the DM and burst width parameter space. Although burst widths up to 100 ms are searched, the completeness of the pipeline drops significantly after ∼30 ms (see Figure 18 of CHIME/FRB Collaboration et al. 2021). This loss in sensitivity occurs because of the fact that CHIME/FRB RFI cleaning algorithms were optimized for short-duration transients and the training data used for the machine learning classifier was biased against the long-duration events (M. Merryfield et al. 2023). The CHIME/Slow pipeline was designed by taking cognizance of these biases and correcting for them and, as a proof-of-concept, to search for second-duration transients using the CHIME telescope.

CHIME/Slow uses a ∼3 bit Huffman compressed intensity data stream copied from the CHIME/FRB 8 bit data stream. This encoding was done as part of a development of another telescope backend: the CHIME All-Sky Multiday Pulsar Stacking Search project (CHAMPSS; The CHAMPSS Collaboration et al. 2025), which searches for pulsars above the period of 10 ms. The factor ∼3 reduction in the intensity data (from 8 bit to 3 bit), the factor of 16 reduction in frequency resolution (from 16,384 channels in case of CHIME/FRB to 1024 channels in case of CHIME/Slow), and the larger than tens of milliseconds time sampling necessary to search for longer timescale transients significantly reduces the computational cost of the CHIME/Slow backend. The downsampling in frequency could impact the search sensitivity for wide low-DM bursts due to intrachannel dispersion smearing. However, other than that, we do not expect any significant loss in sensitivity as the Huffman encoding is lossless and the search is performed at timescales that are comparable to the downsampled time resolution as explained below. The ultimate goal of CHIME/Slow is to systematically search the sky visible to CHIME for radio transients having pulse widths between 16 ms and 5 s.

The CHIME/Slow pipeline is based on well-tested tools that include `PRESTO` (S. Ransom 2011), `HDBSCAN` (L. McInnes et al. 2017) based clustering, and `FETCH` (D. Agarwal et al. 2020). Figure 2 gives an overview of the pipeline showing all major steps. The 3 bit, 0.98304 ms (referred to as 1 ms hereafter) sampled intensity data stream from CHIME/FRB is downsampled to 16, 128, and 512 ms data streams and the search is performed independently on each data stream. The 16 ms data are searched for pulse widths up to 128 ms, the 128 ms data are searched for pulse widths up to 512 ms, and the 512 ms data are searched for pulse widths up to 5 s. RFI cleaning is applied at different stages of the pipeline using different algorithms (see Section 2.2) with parameters optimized to search for long-duration transients. These parameters were fixed by carrying out injections of wide duration bursts into test data using the built-in injection routine and recovering them back with the pipeline. The same routine was also used to estimate the completeness and sensitivity of the current version (see Section 4) and will be used to benchmark the real-time system. The following subsections describe the details of each major block (marked with dotted brown rectangles in the Figure 2) of the pipeline.

2.1. Data Preparation

The first step in the data preparation block is to find and mask RFI channels in the native 3 bit, 1 ms × 1024 frequency channel intensity data (considered as one "chunk"). The masking is performed by computing kurtosis, skew, and standard deviation metrics on the bandpass data and masking the outlier channels. The data are then bandpass corrected and normalized by

subtracting the 1 s chunkwise mean to minimize the effect of gain variations.[25] These data are downsampled to 16, 128, and 512 ms and stored as independent 32 bit filterbank files. The duration of each filterbank file varies based on the downsampling factor to ensure there are enough samples in each file for `PRESTO` to perform time–frequency chunkwise RFI cleaning, dedispersion and single pulse search as explained in the Section 2.2. The 16 ms filterbank file has a duration of ∼1 hr, the 128 ms file has a duration of ∼2 hr and the 512 ms file has a duration of ∼4 hr. Between two consecutive files, an overlap of ∼128 s is included to ensure no transients are missed at the file boundaries. Along with the filterbank files, the bad channel mask computed at the first step is also stored, which is then passed to successive transient search and classification steps.

2.2. Transient Search

The transient search is performed using `PRESTO` to search for single pulses in DM–time space. The transient search block consists of three steps: RFI removal, dedispersion, and single pulse search. The following steps are performed independently for the three time-downsampling factors.

2.2.1. RFI Cleaning

The narrowband, periodic, and impulsive RFI flagging in the time–frequency domain is performed by the `rfifind` routine of `PRESTO`. The input parameters used for the RFI flagging are `clip` = 6, `timesig` = 5, `freqsig` = 15, `chanfrac` = 0.5, `intfrac` = 0.5, and `blocks` = 2, 4, 1 for 16 ms, 12 ms, 512 ms time samplings, respectively. These parameters were qualitatively selected by injecting simulated bursts in test data collected in mid 2022 and maximizing the recovery of the injected bursts after RFI cleaning. A larger injection run was carried out using the standard CHIME/FRB injection routine (M. Merryfield et al. 2023) in 2025 August and the data from this run is being used to optimize the real-time pipeline and measure its selection function. This analysis will be presented in future work.

2.2.2. Dedispersion

The data are dedispersed from DM values of 50–3000 pc cm^{-3} using the `prepsubband` routine of `PRESTO`. The limits on DM search were set based on the available compute in case of the upper limit, while the lower limit was set in order to be mostly sensitivity to extragalactic transients and avoid Galactic sources.[26] For 16 ms time sampling, a DM step of 2 pc cm^{-3} is used, while for 128 and 512 ms time sampling, a DM step of 10 pc cm^{-3} is used. The DM steps were decided using the `DDPlan` routine of `PRESTO`. At this stage, RFI masks computed in the earlier steps (at the data preparation step and by `rfifind`) are used to mask the noisy channels and time blocks, in addition to the zero-DM subtraction,[27] which removes any broadband RFI.

2.2.3. Single Pulse Search

The dedispersed time series are searched for single pulses using the `single_pulse_search.py` routine of `PRESTO`. Boxcar widths of size 2^n are used for the search with the maximum boxcar width determined by the maximum width (`-m`) option of the routine. It is set to 0.13 s, 0.6 s, and 6 s for the 16 ms, 128 ms, and 512 ms time samplings, respectively. The detection threshold is set at a signal-to-noise ratio (S/N) of 10. The single pulse search outputs a file with the DM, time, S/N, and boxcar downfactor (proxy for pulse width) for each detected event. This information is passed to the classification block to identify potential astrophysical events from the RFI.

2.3. Classification

The classification block consists of two main steps: clustering of single pulse events in DM–time parameter space, and identification of FRB-like pulses in the clusters classified as potentially astrophysical. The clustering in DM–time space is performed using the `HDBSCAN` python library. We use `min_cluster_size` and `min_samples` equal to 5 and `cluster_selection_epsilon` of 0.1 for this step. These parameters were selected using the injection analysis (see Section 4) and testing the clustering on real data containing pulsar transits. The selected parameters ensure that events that are sparse with a large distance in the phase space (>0.1 units) are not clustered together, and only densely populated clusters are selected. For each of the remaining clusters, the event with maximum S/N is passed to the `FETCH` classification algorithm to identify whether it is an astrophysical FRB-like event or RFI. For each event, `FETCH` assigns a probability of it being astrophysical in origin. Diagnostic plots are generated for events that have a probability >0.7, as input to the final step of manual classification.[28]

3. CHIME/Slow Pilot Survey

A pilot survey was carried out to test the prototype version of the CHIME/Slow pipeline using the data collected in 2022 December, 2023 January, and 2023 February. These data were collected as part of the development of the CHAMPSS backend. The total on-sky time of these data was 17 days covering ∼13 deg^2 at a given instance as data were collected for only a fraction of 1024 CHIME/FRB beams. The total exposure is equivalent to observing the full CHIME sky for one day (see the Appendix for more details on exposure). The data were searched for single pulses in the dedispersed time series from 16 ms to up to 5 s and for a DM range of 50–3000 pc cm^{-3}.

In this survey, we detect nine bursts (Table 1), which are shown in Figure 3. Out of these nine bursts, one burst, FRB 20230204C, is from a new FRB source and the other eight bursts are from the hyperactive repeater FRB 20220912A (R. McKinven & Chime/Frb Collaboration 2022; A. M. Cook et al. 2024). FRB 20230204C was also detected by CHIME/FRB, but in the side-lobe of neighboring beams, hence exhibiting a narrower bandwidth and pulse width, which enabled its detection as the effective pulse width was in sensitivity range of CHIME/FRB. Out of the eight FRB 20220912A bursts, six bursts were also detected by CHIME/FRB, while two bursts were only detected in CHIME/Slow data.

[25] Similar normalization is also carried out by the CHIME/FRB pipeline.

[26] Note that this choice was made only for the pilot survey, in case of the real-time survey (Section 6), the limits will be revised.

[27] We do not perform any detailed investigation of the effect of zero-DM subtraction on the signal. The main aim of the pilot survey was to detect bright events and zero-DM subtraction is effectively mitigating broadband RFI without significantly affecting the SNR for bright bursts. In the real-time pipeline, we are exploring the possibility of using "flat-fielding," a technique used by D. Kuiper et al. (2026) for the LOFAR telescope. We expect that it will perform better than zero-DM subtraction.

[28] Note that we have not trained `FECTH` on CHIME data yet, and for this analysis we have used the default models.

Table 1
Properties of the Bursts Detected by CHIME/Slow

TNS Name	Arrival Time [a] (UTC)	S/N	DM (pc cm^{-3})	W_{50} (ms)	τ [b] (ms)	z	D_L [c] (Mpc)	Peak Flux (Jy)	Fluence (Jy ms)	Luminosity ($\times 10^{40}$ erg s^{-1})
FRB 20221229A	2022-12-29T00:38:43.030	11.11	223.50 ± 0.31	11.59 ± 1.39	22.55 ± 2.52	$0.0771^{+0.0001}_{-0.0001}$	$361.25^{+0.49}_{--0.49}$	>1.46	>37.51	>1.77
FRB 20221230A	2022-12-30T00:27:01.496	12.73	221.12 ± 0.17	10.22 ± 0.85	9.59 ± 1.42	⋯	⋯	>1.72	>30.43	>2.74
FRB 20230102B	2023-01-02T00:22:45.569	17.88	223.88 ± 0.15	16.44 ± 0.66	⋯	⋯	⋯	>1.21	>21.04	>3.92
FRB 20230102C	2023-01-02T00:23:01.217	14.77	220.50 ± 0.37	25.48 ± 3.16	⋯	⋯	⋯	>0.57	>18.88	>1.22
FRB 20230106D	2023-01-06T23:58:02.322	12.85	222.62 ± 0.20	17.22 ± 0.71	⋯	⋯	⋯	>1.05	>20.06	>1.67
FRB 20230107A	2023-01-07T00:06:08.711	14.58	219.38 ± 0.77	19.73 ± 3.46	75.06 ± 14.89	⋯	⋯	>0.62	>25.45	>2.01
FRB 20230107B	2023-01-07T00:08:04.500	15.93	222.88 ± 0.21	16.08 ± 1.27	11.38 ± 1.89	⋯	⋯	>1.31	>25.36	>2.09
FRB 20230107C	2023-01-07T00:10:48.098	11.48	223.38 ± 0.55	24.47 ± 1.70	⋯	⋯	⋯	>0.76	>23.56	>0.92
FRB 20230204C [d]	2023-02-04T02:41:04.028	16.59	386.25 ± 0.11	3.49 ± 1.32	98.31 ± 8.33	$0.1500^{+0.0800}_{-0.0800}$	$736.92^{+447.10}_{--410.54}$	>0.57	>16.82	>9.57

Notes. The values are estimated using the `fitburst` package and the daily calibration matrices stored by CHIME/FRB. The redshift for FRB 20230204C is estimated using the Macquart relation, and for FRB 20220912A bursts it is taken from V. Ravi et al. (2023). It should be noted that the flux, fluence, and luminosity values reported here are a 3σ lower limits due to the calibration method used in the analysis.

[a] The arrival time is topocentric and at the bottom of the observation band (400 MHz).

[b] Scattering timescale at 400 MHz. A "–" indicates that adding a scattering tail did not improve the fit.

[c] Luminosity distance is estimated assuming a flat-ΛCDM cosmology with the cosmological parameters taken from Planck Collaboration et al. (2020).

[d] The FRB 20230204C is localized to R.A. = $53.^{\circ}02 \pm 0.^{\circ}48$ and decl. = $50.^{\circ}01 \pm 0.^{\circ}48$ by the CHIME/FRB pipeline.

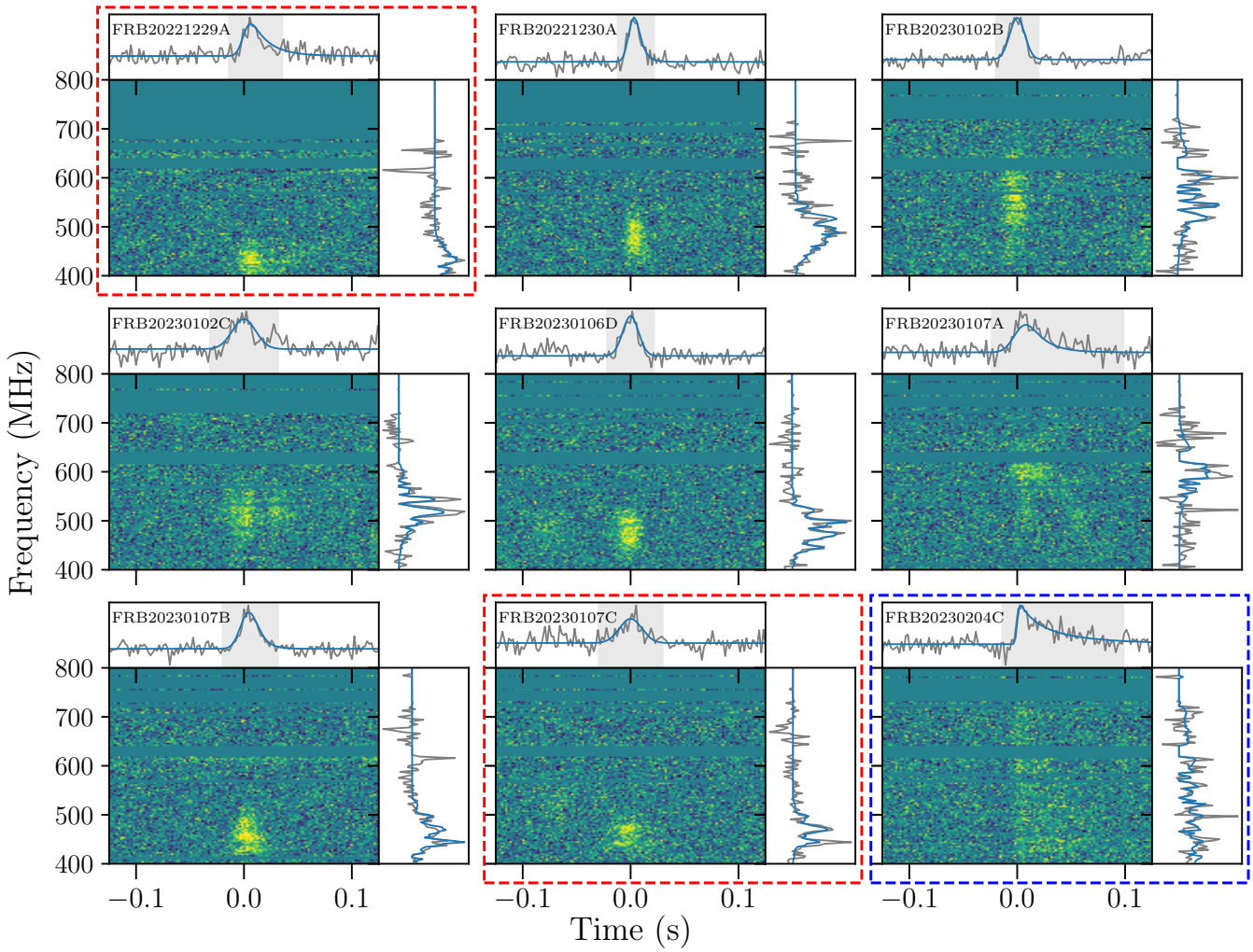

Figure 3. Dynamic spectra ("waterfall" plots), frequency-averaged time series, and time-averaged spectra of bursts detected in the CHIME/Slow pilot survey. The bursts are plotted in order of their arrival times (topocentric) from top left to bottom right. Each plot is corrected for the best-fit DM obtained from `fitburst`. The blue lines in the time profile and spectrum plot show the best-fit frequency-averaged model for the burst profile and time-averaged spectral model estimated over the burst duration, respectively. The last burst, inside the blue box, is the one-off event FRB 20230204C, while all other bursts are from the repeating source FRB 20220912A. Out of these eight bursts, the two marked by red boxes were not detected by CHIME/FRB, while the other six were codetections.

We model the dynamic spectra of each burst using the `fitburst`[29] (E. Fonseca et al. 2024) package. A burst model is least-squares optimized to find the best-fit DM, intrinsic width, scattering timescale (if any), and spectral properties of the burst. We find that adding an exponential scatter-broadening tail[30] to our models improves fits for five out of the nine bursts (for four bursts from FRB 20220912A and FRB 20230204C). We find that FRB 20230204C has an intrinsic width (measured as full-width at half maximum or FWHM) of 3.49 ± 1.32 ms with scattering timescale of 98.31 ± 8.33 ms at 400 MHz, making it one of the most highly scattered FRB detected by CHIME (CHIME/FRB Collaboration et al. 2026). For the eight FRB 20220912A bursts, the intrinsic widths are found to be between 10.22 and 25.48 ms at 400 MHz and the four scattered bursts have scattering timescales between 9.59 and 75.06 ms at 400 MHz.[31]

The DM and intrinsic width values obtained from `fitburst` and the daily calibration metrics stored by CHIME/FRB are used to determine the peak flux of each burst at 1 ms timescale and the total fluence of each burst. We use the same method as described by B. C. Andersen et al. (2023) for the flux/fluence calibration; and hence it should be noted that the flux and fluence values are lower limits as they are not corrected for the actual burst position. The DM information from `fitburst` is used to estimate the redshift of FRB 20230204C by solving for the redshift in the Macquart relation (J. P. Macquart et al. 2020) using the Bayesian Markov Chain Monte Carlo (MCMC) simulations described in Appendix A of M. Bhardwaj et al. (2021). For the FRB 20220912A bursts, we use the redshift reported by V. Ravi et al. (2023). The redshift information is used to estimate luminosity distance and the lower limit on the peak luminosity of all bursts (see Table 1 for all burst properties).

4. Injections and Completeness Analysis

We perform an injection-based completeness analysis to estimate the completeness of the CHIME/Slow pipeline as a

[29] https://github.com/CHIMEFRB/fitburst

[30] We assume a scattering index of −4.

[31] 400 MHz corresponds to the bottom of the CHIME observation band. The widths and scattering timescales are reported at this frequency as `fitburst` reports them at the bottom of the band by default.

Table 2
Injection Parameters Used to Estimate CHIME/Slow Pipeline Completeness

Time Sampling (ms)	DM[a] (pc cm^{-3})	Pulse Width (Intrinsic) (ms)	S/N[b]	Scattering Measure @ 1 GHz (ms)
16	100–3000	1–128	2.12–2376.15	0.001–5
128		120–512	4.52–4776.50	
512		500–4096	4.50–2016.92	

Notes. The S/N values are sampled from a power-law distribution with an index of −1.5. All other values are sampled from a uniform distribution.
[a] We choose 100 pc cm^{-3} as a lower bound for DM as at low DMs we are sensitive to Galactic pulsars. This could cause confusion between a real source and an injected source and we wanted to minimize this effect.
[b] The lower bound of the injected S/N was chosen to be lower than the detection threshold of 10 to account for the fact that the definition of `simpulse` S/N (used for injection) and `PRESTO` S/N (used for detection) are not the same. The expected S/N is also affected by the pulse width, scattering measure, and RFI environment. Hence we sample fainter S/N to ensure we probe the complete parameter space.

function of detection S/N and total injected pulse width (intrinsic + scattering). This is carried out independently on the three data streams (16, 128, and 512 ms). We inject a total of ∼10,000 pulses at each time sampling in ∼4 hr worth of data taken over 10 days and 64 beams. The pulses are injected using the `simpulse`[32] routine over the entire 400–800 MHz band. Table 2 gives the details of injected parameters including the distribution used to sample each parameter. While injecting, we randomize the beam number to sample different directions in the sky. We estimate the completeness at the end of the clustering step by matching the injected pulses with the detected candidates. A candidate is considered recovered when a cluster coincides with the injected pulse in the DM–time parameter space and has a maximum S/N $\geqslant$ 10. The details about estimating the completeness profile are described below.

We bin all injections into total injected pulse width space with 10 ms, 20 ms, and 500 ms binwidths for pulses injected into 16 ms, 128 ms, and 512 ms data, respectively. We evaluated the completeness for each of these bins independently. For each bin, we first bin the data into injected S/N space with width of 0.5 S/N units. Ideally, the detected S/N for each of the injected bins should be close to the injected S/N. Therefore, finding the ratio of total detections of injections ($N_{\rm det}$) to the total injections ($N_{\rm inj}$) in each injected S/N bin should give the completeness profile as a function of detected S/N. However, due to the varying RFI and noise conditions in the data and differences in the total pulse width of each pulse, the detected S/N and injected S/N do not have one-to-one mapping. To account for this, the corresponding detected S/N in each injected S/N bin is determined by taking the median of the detected S/N values for all injections in that bin. The completeness is defined as the fraction $N_{\rm det}/N_{\rm inj}$ for the each of the detected S/N bin defined above.

Figure 4 shows the completeness of CHIME/Slow and CHIME/FRB as a function of detected S/N for a few total injected pulse width bins. Note that the curves are smoothened by fitting a scaled version of the error function to the original data that was obtained following the method described above. It can be seen that CHIME/Slow performs better in recovering

[32] https://github.com/kmsmith137/simpulse

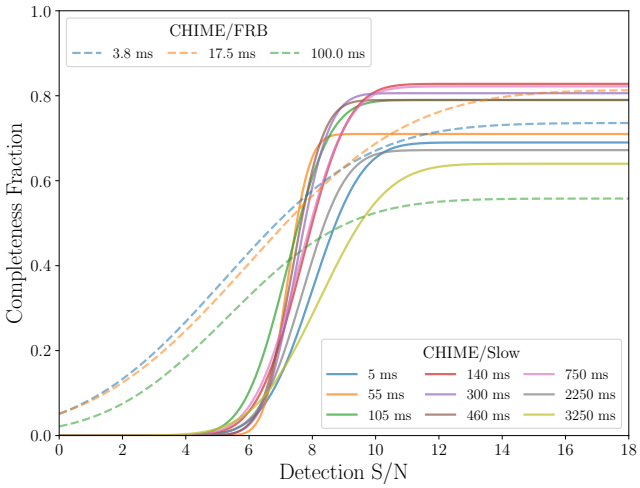

Figure 4. CHIME/Slow and CHIME/FRB completeness as a function of detected S/N for different total (intrinsic + scattering) pulse widths. Only 9 out of the 30 injected pulse width bins are plotted here. The first and the last bin in each column of the legend approximately represent the narrowest and the widest pulse width bin injected in 16 ms, 128 ms, and 512 ms data streams, respectively.

wider bursts. Note that the first CHIME/FRB injection run carried out as part of the Catalog 1 analysis did not include pulses with intrinsic width >100 ms.

5. Estimation of All-sky rate

We use the results from the pilot survey and the completeness analysis to estimate the all-sky rate of radio transients between 16 ms and 5 s. To determine the all-sky rate, we consider the one-off event FRB 20230204C as the only detection and discard the bursts from the repeating FRB 20220912A, as it was hyperactive during the pilot survey and contributed significantly to the all-sky rate of FRBs as shown by O. S. Ould-Boukattine et al. (2025).

The detected rate of transients depends on the intrinsic population model, the sky exposure, and the completeness of the detection pipeline. The intrinsic population model can be a function of multiple parameters (e.g., fluence, width, DM, scattering timescale, etc.), but since we have only one detection, we assume that the intrinsic model only depends on fluence and width and ignore the dependence on other parameters. Also, we consider width as the broadened width, which includes scattering, as completeness analysis was carried out on limited data, making it difficult to disentangle the two effects and constraining our analysis to consider broadened width only. Following this assumption, the observed rate (N^d) of transients between widths $w_{\rm min}$ and $w_{\rm max}$ and fluence $F_{\rm min}$, and between $F_{\rm max}$, is given by:

$$N^d = \int_{w_{\rm min}}^{w_{\rm max}} \int_{F_{\rm min}}^{F_{\rm max}} C(w)E(S)R(F, w; R_0, \beta)dwdF, \qquad (1)$$

where $C(w)$ is the completeness of the pipeline as a function of the width, $E(S)$ is the exposure (sky area × observing time) of the CHIME/Slow data, where the CHIME telescope has a relative sensitivity (with respect to the peak sensitivity under nominal operations and in minimal RFI environment) higher than S, and $R(F, w;R_0, \beta)$ is the intrinsic population model

given by:

$$R(F, w; R_0, \beta) = \frac{-\alpha R_0}{F_0 w_0}\left(\frac{F}{F_0}\right)^{\alpha-1}\left(\frac{w}{w_0}\right)^{\beta}, \quad (2)$$

where, R_0 is the all-sky rate (sky^{-1} day^{-1}) integrated over all fluence and width values, F_0 and w_0 are pivot values for fluence and width, respectively, and α and β are the power-law indices for fluence and width dependence, respectively. The functional form of all-sky rate dependence on fluence is fixed following CHIME/FRB catalog 1 (CHIME/FRB Collaboration et al. 2021) with the assumption that the population is uniformly distributed in a flat Universe, setting the value of α to be –1.5.

For the survey, we had kept our detection threshold at S/N = 10, and hence we compute the completeness and sensitivity for this threshold. We consider a constant value of 0.8 for completeness fraction as, from Figure 4, it can be seen that for most pulse width bins, the completeness is close to this value.[33] The sensitivity S is a function of S/N threshold, fluence, and width and also depends on the beam model and daily sensitivity variations. Details about how the sensitivity and exposure are estimated are given in the Appendix. Here we note that we consider 10% of the peak sensitivity[34] of all beams in our data averaged over frequency, as the cutoff sensitivity and the sky area above this sensitivity is considered for exposure calculation.

We fit the observed rate of one detection in the entire 16 ms to 5 s pulse width range (considered as one bin) with the expected rate given by the Equation (1) using maximum likelihood estimation (MLE) to obtain the all-sky rate R_0. We use binned Poisson likelihood (Particle Data Group et al. 2020) for the MLE estimation, which is given as

$$\ln \mathcal{L} = -\sum_{i}^{M}\left(N_i^e - N_i^d + N_i^d \ln\left[\frac{N_i^d}{N_i^e}\right]\right), \quad (3)$$

where M are the number of bins (one), and N_i^e and N_i^d are the expected and observed numbers of detections in each bin, respectively. The model is fit using MCMC analysis to obtain the posterior distribution of R_0.

For the fitting, we assume a uniform prior in $\log_{10}$ space for R_0 and use three different values of β (–1, –2, and –3) to test the dependence of the rate with respect to three different population models for width. The minimum fluence value is set to 5 Jy ms[35] and the maximum fluence value is set to 100 Jy ms.[36] The parameters F_0 and w_0 in Equation (1) are set to 5 Jy ms and 16 ms, respectively.

We use the `emcee` (D. Foreman-Mackey et al. 2013) package for the MCMC analysis. We marginalize the obtained R_0 posteriors over the three β values. The resulting posterior distribution is shown in Figure 5. As the rate estimation is done on a limited dataset and we only have one detection, we do not report the mean all-sky rate, but instead report the lower and upper limit of the 95% credible region. The estimated all-sky rate of radio transients having widths between 16 ms and 5 s, at observing frequency of 600 MHz and above the fluence of 5 Jy ms is between 184 and 4556 bursts sky^{-1} day^{-1} with 95% confidence.

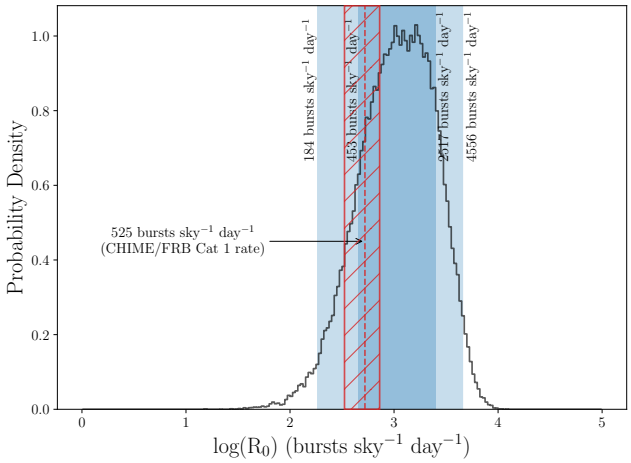

Figure 5. Posterior distribution of the all-sky rate R_0 in log space, marginalized over three different β values (−1, −2, and −3). The light blue and dark blue shaded regions show the 95% and 68% credible interval, respectively. The red vertical dashed line shows the all-sky rate of FRBs estimated by CHIME/FRB Catalog 1 (CHIME/FRB Collaboration et al. 2021) for bursts with fluence above 5 Jy ms and scattering time below 10 ms and the hatched region mark the 95% credible interval for the CHIME/FRB rate.

6. Discussion

The results of the pilot survey demonstrate the capability of CHIME/Slow to detect intrinsically wide as well as highly scattered radio transients and highlight the potential to discover new radio transients in the unexplored parameter space of few hundreds of milliseconds to few seconds. As the pilot survey was a proof-of-concept that was only later converted into a real-time pipeline, there is significant scope for modifications in the pipeline described here to improve the sensitivity and optimize the processing speed. Some of these improvements include better RFI mitigation strategies (e.g., subtracting the average over neighboring beams; D. Kuiper et al. 2026), optimization of the clustering parameters and multibeam clustering to reduce false positives, retraining `FETCH` on the already collected CHIME/Slow data to improve the classification accuracy, improvements to the code efficiency to reduce the processing time, and more systematic injection analyses to better characterize the sensitivity and completeness of the pipeline.

These optimization efforts are currently underway in parallel to running the current version of the pipeline as a real-time backend at the CHIME site with partial operations.[37] When fully operational, the real-time CHIME/Slow backend will be capable of searching the entire CHIME sky in real-time for radio transients between 16 ms and 5 s pulse widths, with a low-latency alert system to report detected transients to the community (e.g., via the `frb-voe` service, T. C. Abbott et al. 2025). Description of the real-time CHIME/Slow backend and

[33] Note that the injection analysis was done on a limited amount of data and hence we have not truly sampled the intrinsic noise properties. Therefore taking a constant and more conservative value of 0.8 for the completeness fraction is a safe assumption, as it will only lead to an underprediction of the all-sky rate.

[34] The peak sensitivity is attained at the zenith of the beam.

[35] This value is chosen to match the CHIME/FRB Catalog 1 fluence threshold (CHIME/FRB Collaboration et al. 2021).

[36] This is chosen to be arbitrarily high such that a burst of this fluence will be detectable by CHIME at a very low sensitivity as well.

[37] We are searching about ∼300 beams out of the 1024 CHIME/FRB beams since 2025 October.

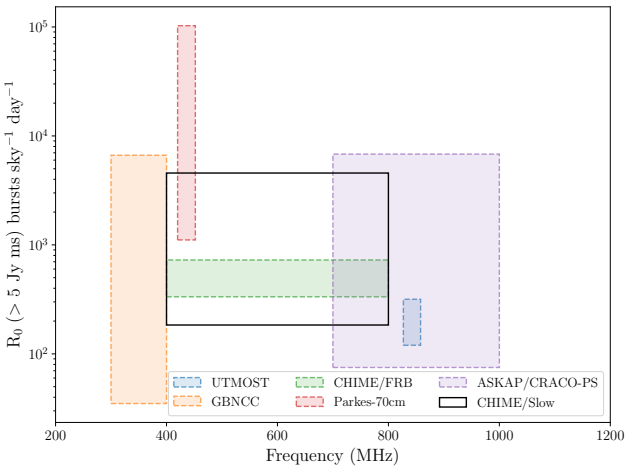

Figure 6. CHIME/Slow pilot survey all-sky rate of radio transients plotted along with the all-sky rate estimated by other surveys with center frequencies close to CHIME. All the rates are scaled to the CHIME/Slow and CHIME/FRB fluence threshold of 5 Jy ms assuming a Euclidean distribution of sources (i.e., $N(>F) \propto F^{-1.5}$). The data are taken from W. Farah et al. (2019; UTMOST), E. Parent et al. (2020; GBNCC), CHIME/FRB Collaboration et al. (2021; CHIME/FRB), F. Crawford et al. (2022), Z. Wang et al. (2025; Parkes-70cm), and Z. Wang et al. (2025; ASKAP/CRACO). Note that the Parks-70 cm value reported here is the reestimation of the original rate by Z. Wang et al. (2025) and not the rate reported by F. Crawford et al. (2022).

results from the real-time survey will be presented in a future work.

Figure 6 shows the estimated all-sky rate from the CHIME/Slow pilot survey along with the all-sky rates estimated by other surveys at similar frequencies. From the figure, it can be seen that the CHIME/Slow pilot survey rate estimate is comparable to the rates estimated by other surveys, except for the upper limit of Parkes-70 cm survey (F. Crawford et al. 2022), which is an order of magnitude higher than any other estimates. This value is a reestimation of the original rate by Z. Wang et al. (2025) by considering only one out of four detections reported by F. Crawford et al. (2022) to be of astrophysical origin.[38] The original rate reported by F. Crawford et al. (2022) is significantly higher and is inconsistent with other survey rates. Consistent estimates on all-sky rates between CHIME/Slow and other surveys, particularly the ASKAP/CRACO-PS and Parkes-70 cm in which pulse widths up to ∼200 ms were searched, clearly highlight the prediction that most current surveys, tuned mostly for millisecond-duration FRBs, could be missing a population of intrinsically wide and/or highly scattered FRBs. Hence, in addition to CHIME/Slow, the ongoing efforts by many other telescopes to search for wider duration radio transients are well placed to uncover this missing population.

One caveat to note while comparing the rates from different surveys with the rate predicted by the CHIME/Slow pilot survey is that the maximum duration and DM searched in these surveys are different compared to our survey. The CHIME/Slow pilot survey searched up to 5 s pulse widths and up to DM of 3000 pc cm^{-3}, while the maximum pulse width searched in other surveys is ∼200 ms; however, other surveys have searched much larger DMs (up to ∼13,000 pc cm^{-3} in case of CHIME/FRB and ASKAP/CRACO-PS). Although, we do not expect our rate estimate to change significantly if we had searched for higher DMs as preliminary checks with injection data did not show a lack of completeness at high DMs. To quantify the dependence of the rate on DM and on pulse widths, particularly $\gtrsim$1 s, more detections are necessary. Future work with a larger sample of detected transients from the real-time CHIME/Slow survey will help to better understand the pulse width and DM dependence and constrain the all-sky rate more accurately.

When comparing the CHIME/Slow pilot survey results with CHIME/FRB Catalog 1 (CHIME/FRB Collaboration et al. 2021) and injection system results (M. Merryfield et al. 2023), the prediction by both works that CHIME/FRB could be missing highly scattered bursts is strongly supported by this work. The pilot survey has already detected one of the most highly scattered bursts by the CHIME telescope, and the all-sky rate predicted by the pilot survey is consistent with the CHIME/FRB all-sky rate supporting the hypothesis that there is an undetected population of highly scattered events in the CHIME/FRB data. The CHIME/Slow real-time pipeline will detect more such highly scattered bursts in the future, which will be crucial to understand the local burst environments. These predictions, the results, and the lessons learnt from the systematic CHIME/Slow real-time survey will be crucial to guide any future upgrades to the CHIME telescope to incorporate wider pulse width searches and also to guide any future surveys.

7. Conclusions

The discovery of FRBs prompted the development of new search techniques to systematically search for FRB-like radio transients. However, due to some technological limitations (e.g., RFI mitigation algorithms), these searches have been limited to millisecond-duration transients, and wider pulse widths have been largely unexplored. Recent discoveries of long-period radio transients, as well as some theoretical predictions of FRB-like radio transients associated with compact binary mergers and GRBs, highlight the potential of a systematic search for second-duration radio transients. The CHIME/Slow backend attempts to fill this unexplored parameter space by systematically searching for radio transients with 16 ms–5 s pulse widths.

In this article, we have described the prototype version of the CHIME/Slow pipeline and results from the CHIME/Slow pilot survey carried out using archival data. The CHIME/Slow pipeline is based on well-tested tools such as `PRESTO`, `HDBSCAN`, and `FETCH` and has a built-in injection routine to benchmark its performance. The pipeline was tested on archival data collected in 2022 December and 2023 January and 2023 February. In these data, nine bursts were detected, one of which is a new nonrepeating FRB and eight are from a hyperactive known repeater. We also report the lower and upper limit (95% credible region) on the all-sky rate of radio transients with pulse widths between 16 ms and 5 s, at observing frequency of 600 MHz, and fluence threshold of 5 Jy ms to be 184 and 4556 bursts sky^{-1} day^{-1}

The CHIME/Slow pilot survey pipeline is being ported to run as a real-time backend at the CHIME site. The backend is already partially online in its current version, and efforts are underway to optimize the pipeline for real-time operations and to scale the system to handle the full CHIME sky. We expect to have the real-time CHIME/Slow backend fully operational by mid to late 2026.

[38] Two of the remaining three detections have low S/N and one has a narrow bandwidth in an already band-limited data (total bandwidth of 32 MHz) making the candidates marginal.

Acknowledgments

We acknowledge that CHIME is located on the traditional, ancestral, and unceded territory of the Syilx/Okanagan people. We are grateful to the staff of the Dominion Radio Astrophysical Observatory, which is operated by the National Research Council of Canada. CHIME is funded by a grant from the Canada Foundation for Innovation (CFI) 2012 Leading Edge Fund (Project 31170) and by contributions from the provinces of British Columbia, Québec, and Ontario. The CHIME/FRB Project is funded by a grant from the CFI 2015 Innovation Fund (Project 33213) and by contributions from the provinces of British Columbia and Québec, and by the Dunlap Institute for Astronomy and Astrophysics at the University of Toronto.

CHIME/Slow is supported by Dunlap seed funding provided by the Dunlap Institute. The Dunlap Institute is funded through an endowment established by the David Dunlap family and the University of Toronto.

We thank Parag Shah from TIFR for the help in setting up the compute node on which the pilot survey was carried out. We are grateful to Scott Ransom for his input on configuring `PRESTO` to make it compatible with CHIME/Slow data. We thank Natasha Hurley-Walker, Manisha Caleb, and Iris de Ruiter for sharing the data for Figure 1 and Andy Wang for sharing the data for Figure 6.

Z.P. is supported by an NWO Veni fellowship (VI. Veni.222.295). P.S. acknowledges the support of an NSERC Discovery Grant (RGPIN-2024-06266). F.A.D. was supported by an NRAO Jansky Fellowship, F.A.D. is supported by an NRC SKA Fellowship. The AstroFlash research group at McGill University, University of Amsterdam, ASTRON, and JIVE is supported by a Canada Excellence Research Chair in Transient Astrophysics (CERC-2022-00009); an Advanced Grant from the European Research Council (ERC) under the European Union's Horizon 2020 research and innovation program ("EuroFlash;" grant agreement No. 101098079); and an NWO-Vici grant ("AstroFlash;" VI.C.192.045). V.M.K. holds the Lorne Trottier Chair in Astrophysics & Cosmology, a Distinguished James McGill Professorship, and receives support from an NSERC Discovery grant (RGPIN 228738-13). K.N. acknowledges support by NASA through the NASA Hubble Fellowship grant # HST-HF2-51582.001-A awarded by the Space Telescope Science Institute, which is operated by the Association of Universities for Research in Astronomy, Incorporated, under NASA contract NAS5-26555. FRB and Pulsar research at UBC is supported by an NSERC Discovery Grant and by the Canadian Institute for Advanced Research.

Software: NumPy (C. R. Harris et al. 2020), SciPy (P. Virtanen et al. 2020), Matplotlib (J. D. Hunter 2007), Astropy (Astropy Collaboration et al. 2022), PRESTO (S. Ransom 2011), HDBSCAN (L. McInnes et al. 2017), FETCH (D. Agarwal et al. 2020), emcee (D. Foreman-Mackey et al. 2013).

Appendix
Exposure Calculation

Here we explain the details of the exposure calculation necessary to forward-model the all-sky rate following Equation (1). The exposure depends on the CHIME/FRB beam model, the daily sensitivity variations, and the daily observing time. First, we define a relative sensitivity metric (S), for a given intrinsic width (w) and fluence (F), as the minimum sensitivity required to detect a burst above the S/N threshold of $\mathrm{S/N_{thr}} = 10$. This sensitivity is defined as:

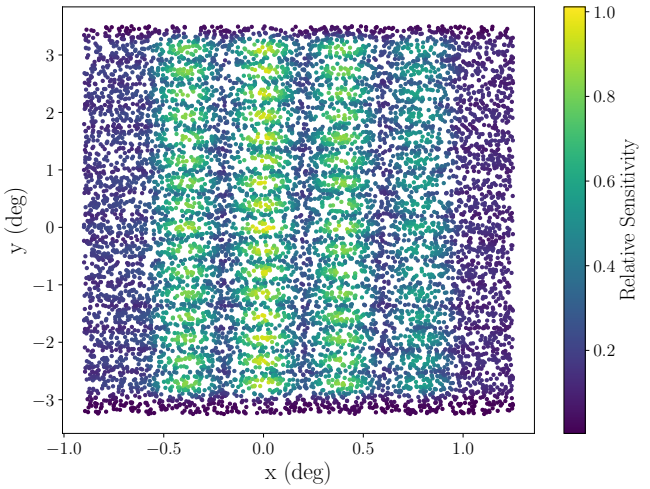

Figure A1. Relative sensitivity as a function of sky position for all 64 beams in the CHIME/Slow data. The X and Y axes represent angles in telescope coordinates, and are aligned in the north–south and east–west directions, respectively.

$$S = \frac{\mathrm{S/N_{thr}}}{\mathrm{S/N_{max}}}, \tag{A1}$$

where $\mathrm{S/N_{max}}$ is the maximum S/N of a burst with fluence F and width w at the peak sensitivity of the CHIME beam (i.e., at zenith, under nominal operations with no excess RFI). The $\mathrm{S/N_{max}}$ is computed using the radiometer equation following P. Chawla et al. (2017) as:

$$\mathrm{S/N_{max}} = \frac{fGw}{\beta(T_{\mathrm{sys}} + T_{\mathrm{sky}})}\sqrt{\frac{n_p \Delta\nu}{w_b}}, \tag{A2}$$

where f is the flux density of the burst (F/w_b), G is the telescope gain at zenith, w is the intrinsic width (including scattering) of the burst, β is a factor to account for the digitization loss, T_{sys} and T_{sky} are the system and sky temperatures, respectively, n_p is the number of polarizations summed, $\Delta\nu$ is the bandwidth, and w_b is the broadened width. Since we do not differentiate between the intrinsic width and scattering in our analysis, the definition of broadened width is given by:

$$w_b = \sqrt{w_i^2 + t_{\mathrm{samp}}^2 + t_{\mathrm{DM}}^2}, \tag{A3}$$

where t_{samp} is the sampling time and t_{DM} is the intrachannel DM smearing time.

We use typical values from CHIME/FRB for the parameters in the radiometer equation, with $G = 1.38$ K Jy^{-1}, $\beta = 1.0$, $T_{\mathrm{sys}} = 50$ K, $n_p = 2$, and $\Delta\nu = 200$ MHz (accounting for about 50% loss in the number of channels due to the RFI masking). The sky temperature, $T_{\mathrm{sky}} = 10$ K, is estimated by extrapolating (with spectral index of –2.6) the reprocessed Haslam 408 MHz sky temperature map (M. Remazeilles et al. 2015) to the CHIME central frequency of 600 MHz, and taking the average value over the observed part of the sky. When computing the broadened width and intrinsic width, as mentioned in Section 5, we consider w to include scattering effects, and hence the broadened width only includes the

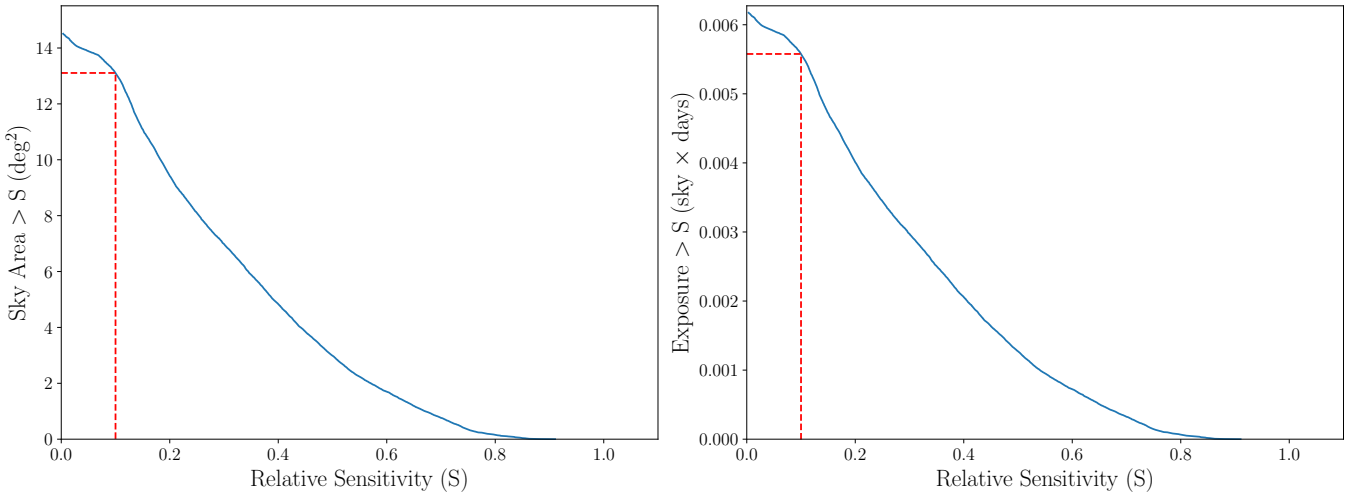

Figure A2. Left: sky area (in deg^2) above the relative sensitivity of S. The horizontal and vertical lines mark the area above the 10% relative sensitivity threshold used for the exposure calculation. This area corresponds to 13.10 deg^2. Right: the total exposure (sky × days) above the relative sensitivity S. The horizontal and vertical lines mark the total exposure above the 10% relative sensitivity threshold.

sampling time as we ignore the intrachannel DM smearing, since contribution from it is minimal at typical DMs.

As mentioned in Section 5, the exposure ($E(S)$, sky area × observing time, see Equation (1)) is estimated assuming a relative sensitivity of 10% of the peak sensitivity. Assuming this, we first estimate the cumulative sky fraction visible above this threshold sensitivity to all 64 beams for which the CHIME/Slow pilot survey data was collected. The CHIME/FRB beam model gives the sensitivity of each beam for a point on the sky relative to the zenith as a function of frequency.[39] To estimate the cumulative sky fraction, we first randomly sample the sky in the east–west and north–south directions centered at telescope meridian, and only covering the sky area corresponding to the 16 beam rows, and find frequency-averaged sensitivity for each beam at each position using the beam model. Then for each position in the sky, we take the maximum of the sensitivities over the beams, and consider that value as the sensitivity of the telescope at that position (see Figure A1).

We then assume that the total area of each sampled point is dA, which is given by A/N, where A is the total area sampled and N is the number of points sampled. To calculate the cumulative sky fraction above 10% relative sensitivity, we sort the sensitivities and take the cumulative sum of the area. This is further corrected for the daily sensitivity variations by multiplying the sensitivities with the daily sensitivity factor and then finding the sky area corresponding to the corrected 10% sensitivity. The daily sensitivity factor is estimated based on the total number of pulsars detected by CHIME/FRB in a day compared with the expected number of pulsars detections under nominal operating conditions. The corrected cumulative sky area above the relative sensitivity of 10% is shown in Figure A2 (left). This area is then converted to the daily exposure by finding the fraction of the sky that is visible per day and multiplying that with the total number of observing days. Figure A2 (right) shows the exposure as a function of relative sensitivity. The exposure is then used in Equation (1) to estimate the observed rate of transients.

[39] For details regarding CHIME/FRB beams and their orientation, see CHIME/FRB Collaboration et al. (2021).

ORCID iDs

Sujay Mate https://orcid.org/0000-0001-5536-4635
Kevin Luke https://orcid.org/0000-0003-4443-4508
Yash Bhusare https://orcid.org/0000-0002-5342-163X
Arvind Balasubramanian https://orcid.org/0000-0003-0477-7645
Ziggy Pleunis https://orcid.org/0000-0002-4795-697X
Paul Scholz https://orcid.org/0000-0002-7374-7119
Shriharsh P. Tendulkar https://orcid.org/0000-0003-2548-2926
Mohit Bhardwaj https://orcid.org/0000-0002-3615-3514
Charanjot Brar https://orcid.org/0000-0002-1800-8233
Fengqiu Adam Dong https://orcid.org/0000-0003-4098-5222
Emmanuel Fonseca https://orcid.org/0000-0001-8384-5049
B. M. Gaensler https://orcid.org/0000-0002-3382-9558
Jason Hessels https://orcid.org/0000-0003-2317-1446
Jeff Huang https://orcid.org/0000-0002-8043-0048
Naman Jain https://orcid.org/0009-0009-0938-1595
Ronniy C. Joseph https://orcid.org/0000-0003-3457-4670
Victoria M. Kaspi https://orcid.org/0000-0001-9345-0307
Afrokk Khan https://orcid.org/0009-0004-4176-0062
Robert Main https://orcid.org/0000-0002-7164-9507
Bradley W. Meyers https://orcid.org/0000-0001-8845-1225
Nikola Milutinovic https://orcid.org/0000-0001-8292-0051
Kenzie Nimmo https://orcid.org/0000-0003-0510-0740
Kaitlyn Shin https://orcid.org/0000-0002-6823-2073
David Spear https://orcid.org/0009-0003-6054-8035
Ingrid Stairs https://orcid.org/0000-0001-9784-8670
Chia Min Tan https://orcid.org/0000-0001-7509-0117

References

Abbott, T. C., Zwaniga, A. V., Brar, C., et al. 2025, AJ, 169, 39
Agarwal, D., Aggarwal, K., Burke-Spolaor, S., Lorimer, D. R., & Garver-Daniels, N. 2020, MNRAS, 497, 1661
Andersen, B. C., Patel, C., Brar, C., et al. 2023, AJ, 166, 138
Anderson, M. M., Hallinan, G., Eastwood, M. W., et al. 2018, ApJ, 864, 22
Astropy Collaboration, Price-Whelan, A. M., Lim, P. L., et al. 2022, ApJ, 935, 167
Bhardwaj, M., Kirichenko, A. Y., Michilli, D., et al. 2021, ApJL, 919, L24
Caleb, M., Heywood, I., Rajwade, K., et al. 2022, NatAs, 6, 828

Caleb, M., Lenc, E., Kaplan, D. L., et al. 2024, NatAs, 8, 1159
Chastain, S. I., van der Horst, A. J., Rowlinson, A., et al. 2023, MNRAS, 526, 1888
Chawla, P., Kaspi, V. M., Josephy, A., et al. 2017, ApJ, 844, 140
CHIME/FRB Collaboration, Abbott, T., Andersen, B. C., et al. 2026, ApJS, 283, 34
CHIME/FRB Collaboration, Amiri, M., Andersen, B. C., et al. 2021, ApJS, 257, 59
CHIME/FRB Collaboration, Amiri, M., Bandura, K., et al. 2018, ApJ, 863, 48
Cook, A. M., Scholz, P., Pearlman, A. B., et al. 2024, ApJ, 974, 170
Cordes, J. M., Lazio, T. J. W., & McLaughlin, M. A. 2004, NewAR, 48, 1459
Crawford, F., Hisano, S., Golden, M., et al. 2022, MNRAS, 515, 3698
Curtin, A. P., Sirota, S., Kaspi, V. M., et al. 2024, ApJ, 972, 125
Curtin, A. P., Tendulkar, S. P., Josephy, A., et al. 2023, ApJ, 954, 154
de Ruiter, I., Rajwade, K. M., Bassa, C. G., et al. 2025, NatAs, 9, 672
Dong, F. A., Clarke, T. E., Curtin, A., et al. 2025, ApJL, 990, L49
Farah, W., Flynn, C., Bailes, M., et al. 2019, MNRAS, 488, 2989
Fonseca, E., Pleunis, Z., Breitman, D., et al. 2024, ApJS, 271, 49
Foreman-Mackey, D., Hogg, D. W., Lang, D., & Goodman, J. 2013, PASP, 125, 306
Harris, C. R., Millman, K. J., van der Walt, S. J., et al. 2020, Natur, 585, 357
Hennessy, A., Starling, R. L. C., Rowlinson, A., et al. 2023, MNRAS, 526, 106
Hunter, J. D. 2007, CSE, 9, 90
Hurley-Walker, N., Rea, N., McSweeney, S. J., et al. 2023, Natur, 619, 487
Hurley-Walker, N., Zhang, X., Bahramian, A., et al. 2022, Natur, 601, 526
Keane, E. F. 2018, NatAs, 2, 865
Kuiper, D., Bassa, C., Pleunis, Z., & Hessels, J. 2026, arXiv:2603.12970
Lyutikov, M. 2024, arXiv:2402.16504
Macquart, J. P., Prochaska, J. X., McQuinn, M., et al. 2020, Natur, 581, 391
McInnes, L., Healy, J., & Astels, S. 2017, JOSS, 2, 205
McKinven, R. & Chime/Frb Collaboration 2022, ATel, 15679, 1
Merryfield, M., Tendulkar, S. P., Shin, K., et al. 2023, AJ, 165, 152
Ould-Boukattine, O. S., Chawla, P., Hessels, J. W. T., et al. 2025, MNRAS, 545, staf1937
Parent, E., Chawla, P., Kaspi, V. M., et al. 2020, ApJ, 904, 92
Particle Data Group, Zyla, P. A., Barnett, R. M., et al. 2020, PTEP, 2020, 083C01
Planck Collaboration, Aghanim, N., Akrami, Y., et al. 2020, A&A, 641, A6
Ransom, S. 2011, PRESTO: PulsaR Exploration and Search TOolkit, Astrophysics Source Code Library, ascl:1107.017
Ravi, V., Catha, M., Chen, G., et al. 2023, ApJL, 949, L3
Remazeilles, M., Dickinson, C., Banday, A. J., Bigot-Sazy, M.-A., & Ghosh, T. 2015, MNRAS, 451, 4311
Rowlinson, A., & Anderson, G. E. 2019, MNRAS, 489, 3316
Rowlinson, A., Gourdji, K., van der Meulen, K., et al. 2019, MNRAS, 490, 3483
Rowlinson, A., Starling, R. L. C., Gourdji, K., et al. 2021, MNRAS, 506, 5268
Sridhar, N., Zrake, J., Metzger, B. D., Sironi, L., & Giannios, D. 2021, MNRAS, 501, 3184
Starling, R. L. C., Rowlinson, A., van der Horst, A. J., & Wijers, R. A. M. J. 2020, MNRAS, 494, 5787
The CHAMPSS Collaboration, Andrade, C., Boyle, P. J., et al. 2025, ApJ, 990, 50
Tian, J., Anderson, G. E., Hancock, P. J., et al. 2022, MNRAS, 514, 2756
Usov, V. V., & Katz, J. I. 2000, A&A, 364, 655
Virtanen, P., Gommers, R., Oliphant, T. E., et al. 2020, NaMet, 17, 261
Wang, Z., Bannister, K. W., Gupta, V., et al. 2025, PASA, 42, e005